



Evidence of hotspot paths below Arabia and the Horn of Africa and consequences on the Red Sea opening



S. Vicente de Gouveia^{a,*}, J. Besse^a, D. Frizon de Lamotte^b, M. Greff-Lefftz^a, M. Lescanne^c, F. Gueydan^d, F. Leparmentier^e

^a Institut de Physique du Globe de Paris - Sorbonne Paris Cité, Université Paris Diderot, UMR CNRS 7154, 1 rue Jussieu, 75252 Paris 05, France

^b Département Géosciences et Environnement, Université de Cergy-Pontoise, Cergy-Pontoise, France

^c Total EP, Pau, France

^d Géosciences Montpellier, Université de Montpellier, CNRS UMR 5243, Montpellier, France

^e Total EP, Paris La Défense, France

ARTICLE INFO

Article history:

Received 11 December 2017

Received in revised form 25 January 2018

Accepted 29 January 2018

Available online xxxxx

Editor: R. Bendick

Keywords:

hotspot
hotspot reference frame
heat-flow
rifting
Red Sea

ABSTRACT

Rifts are often associated with ancient traces of hotspots, which are supposed to participate to the weakening of the lithosphere. We investigated the expected past trajectories followed by three hotspots (Afar, East-Africa and Lake-Victoria) located around the Red Sea. We used a hotspot reference frame to compute their location with respect to time, which is then compared to mantle tomography interpretations and geological features. Their tracks are frequently situated under continental crust, which is known to strongly filter plume activity. We looked for surface markers of their putative ancient existence, such as volcanism typology, doming, and heat-flow data from petroleum wells. Surface activity of the East-Africa hotspot is supported at 110 Ma, 90 Ma and 30 Ma by uplift, volcanic activity and rare gas isotopic signatures, reminiscent of a deep plume origin. The analysis of heat-flow data from petroleum wells under the Arabian plate shows a thermal anomaly that may correspond to the past impact of the Afar hotspot. According to derived hotspot trajectories, the Afar hotspot, situated (at 32 Ma) 1000 km north-east of the Ethiopian–Yemen traps, was probably too far away to be accountable for them. The trigger of the flood basalts would likely be linked to the East-Africa hotspot. The Lake-Victoria hotspot activity appears to have been more recent, attested only by Cenozoic volcanism in an uplifted area. Structural and thermal weakening of the lithosphere may have played a major role in the location of the rift systems. The Gulf of Aden is located on inherited Mesozoic extensional basins between two weak zones, the extremity of the Carlsberg Ridge and the present Afar triangle, previously impacted by the East-Africa hotspot. The Red Sea may have opened in the context of extension linked to Neo-Tethys slab-pull, along the track followed by the East Africa hotspot, suggesting an inherited thermal weakening.

© 2018 Elsevier B.V. All rights reserved.

1. Introduction

Hotspots are the surface expression of mantle thermal instabilities, which arise from high temperature and low viscosity zones. Their activity is revealed by surface and subsurface phenomena, such as volcanic traps, or chains of volcanoes on oceanic floor. A thin conduit with a spherical head (Olson et al., 1988) characterises hotspots in laboratory experiments and numerical sim-

ulations. Traps, which are the most common continental volcanism linked to hotspots (Courtillot et al., 2003), would result from an impingement under the lithosphere of a plume head (about 1000 km wide), while hotspot tracks on the ocean floor, result from impingement of a plume conduit (about 100 km wide). The present resolution of seismic tomography is insufficient to precisely image objects of this size, although some interpretations may display conduits as large as 300 to 500 km wide (French and Romanowicz, 2015).

Hotspot activity is episodic and irregular, as shown by the discontinuously spaced volcanic edifices on oceanic hotspot tracks, while the track itself has a finite duration of tens to hundreds of millions of years. Based on laboratory experiments and observations, Davaille et al. (2005) showed that hotspot activity is episodic, and computed a recurrence time range between 100 and 180 Myr.

* Corresponding author.

E-mail addresses: vicente@ipgp.fr (S. Vicente de Gouveia), besse@ipgp.fr (J. Besse), Dominique.Frizon-de-Lamotte@u-cergy.fr (D. Frizon de Lamotte), greff@ipgp.fr (M. Greff-Lefftz), marc.lescanne@total.com (M. Lescanne), frederic.gueydan@umontpellier.fr (F. Gueydan), francois.leparmentier@total.com (F. Leparmentier).

Table 1
Afar, East-Africa and Lake-Victoria hotspot coordinates, according to several studies.

Hotspot name – Coordinates			Reference
Afar (10°; 42°)	East-Africa (6°; 34°)	Lake-Victoria (–3°; 34°)	Burke and Wilson, 1976 ^a
Afar (10°; 42°)	East-Africa (6°; 34°)	Lake-Victoria (–3°; 34°)	Thiessen et al., 1979 ^a
Ethiopia (10°; 43°)	–	East-Africa (–3°; 38°)	Crough, 1983 ^a
Afar/Ethiopia (12°; 42°)	–	Lake-Victoria/East-Africa (–3°; 36°)	Richards et al., 1988 ^b
–	East-Africa (6°; 34°)	–	Steinberger, 2000 ^b
Afar (10°; 43°)	–	–	Courtillot et al., 2003 ^b
Afar (7°; 39°)	–	Lake-Victoria (–3°; 38°)	Montelli et al., 2006 ^b
Afar (7°; 39°)	East-Africa (6°; 34°)	Lake-Victoria (–3°; 38°)	Ritsema et al., 2011 ^c
Afar (12°; 42°)	East-Africa (6°; 34°)	Lake-Victoria (–3°; 38°)	This study

^a Hotspots coordinates determined from a map georeferencing.

^b Hotspot coordinates from datasets.

^c Hotspot location derived from tomographic model images.

Thanks to oceanic tracers, it is possible to directly assess the duration of hotspot activity. For instance, Clouard and Bonneville (2001) highlighted that the Louisville hotspot could have formed the Ontong Java Plateau at about 121–124 Ma, and the oceanic seamounts between 66 and 12.5 Ma. Therefore, the Louisville hotspot activity could have had a lifetime of 100 Myr.

With the exception of continental flood basalts, the knowledge of hotspot effects on the continental lithosphere remains poor, and their tracks are particularly difficult to evidence, as the lithospheric thickness filters their surface effects. However, Chu et al. (2013) observed a hotspot track under the North American continental lithosphere, using seismological data. Also, Davies et al. (2015) cross-correlated the episodic volcanism in eastern Australia with the Cosgrove hotspot track, in regions where the lithosphere is thin.

In this study, we investigated the history of three hotspots of the East African area, widely described in the literature, namely Afar, East-Africa and Lake-Victoria, with the aim of retrieving traces of their ancient activity. In addition, we highlight new considerations and questions about the Red Sea rift system, which is superimposed on the East-Africa hotspot trajectory.

2. Hotspot tracks in the Arabian plate and the Horn of Africa

We aimed to retrieve the path followed by three hotspots. All are currently situated in Eastern Africa – Afar, East-Africa and Lake-Victoria. To do that, we first described the geological setting of the studied area, then defined the present day hotspot coordinates, using various lines of evidence, and finally, following a comparative hotspot reference frame study, we used the more accurate reference frame to derive the expected hotspot paths for the last 110 Myr.

2.1. Geological context

During the Neoproterozoic, the Pan-African orogeny led to the formation of the Arabian–Nubian Shield through the amalgamation of microcontinents and arcs (Fritz et al., 2013). Then, Arabia and Africa moved together, before splitting at the end of the Miocene. The rifting started during the Oligocene, occurring along two rift systems – the Red Sea and the Gulf of Aden (e.g., Bellahsen et

al., 2003). It is generally considered that the trigger of the rifting were the tectonic forces related to the Neo-Tethys slab-pull and the subsequent subcontinental mantle delamination, combined with a hotspot impact that thermally weakened the lithosphere in the Afar region (Zeyen et al., 1997; Bellahsen et al., 2003; Faccenna et al., 2013; Autin et al., 2013). Different scenarios have been proposed for the Red Sea rifting and drifting since the Ethiopian–Yemen traps emplacement (Bosworth et al., 2005; Almalki et al., 2014); however, all of them converge to consider a drifting onset at 5 Ma. The Red Sea rift developed from the Afar region northeastward. By contrast, the Gulf of Aden opening started east of the Gulf of Aden from the Carlsberg Ridge, propagating westward, through the Sheba Ridge, at 17.6 Ma, and the Aden Ridge from ~10 Ma onward (Bosworth et al., 2005; Fournier et al., 2010; Leroy et al., 2012).

2.2. Hotspot present day locations

In the literature, the names of the three hotspots may refer to different volcanic activities, or suspected plumes, in space and time. For example, the ‘Afar hotspot’ is considered to correspond to the plume that generated the Ethiopian–Yemen traps (see Courtillot et al., 2003), while its present location is associated with the Stratoid Series volcanism (see Stab et al., 2016) and with tomographic studies (Montelli et al., 2006). On the contrary, the ‘Afar hotspot’ in French and Romanowicz (2015), located at 6°N, 34°E, clearly refers to the ‘East-Africa hotspot’. A review of the present day coordinates and hotspot names of several authors is, thus, given in Table 1. We considered the following three hotspots, using related traps and tomographic images (Table 1):

(1) The Afar hotspot (see review in Stab et al., 2016) is defined by the Stratoid Series at 4 Ma, and by tomographic interpretation of a large low-velocity anomaly below the Afar triple junction (12°N, 42°E).

(2) The East-Africa hotspot’s present position is indirectly established from the mean position of the Ethiopian–Yemen traps, as suggested by Steinberger (2000). We determined the mean position of these traps at 30 Ma, assuming that the relative hotspot was located in the mantle vertically from the mean traps position. Then, using O’Neill et al.’s (2005) hotspot reference frame (see Section 2.3), we computed the current position of the mean traps

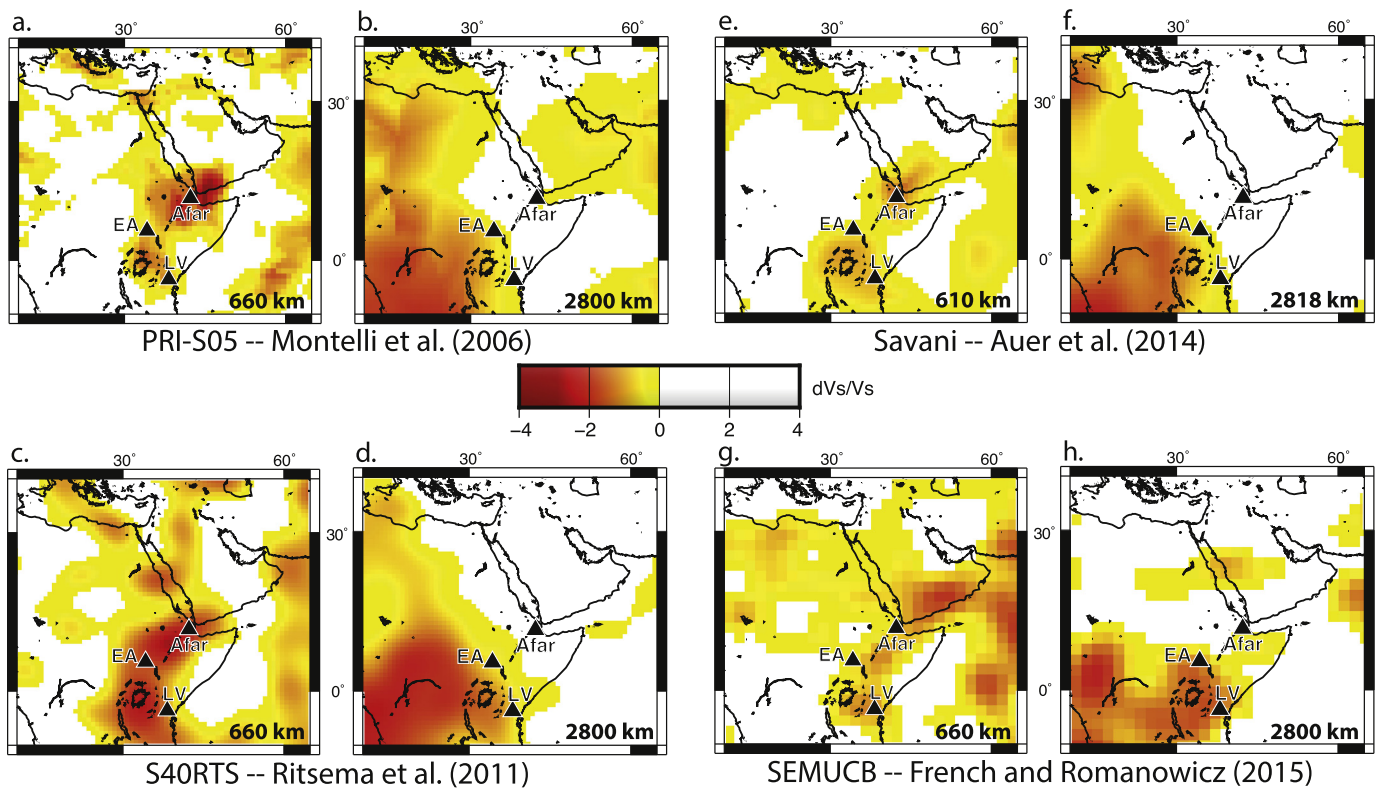


Fig. 1. Tomographic images derived from four different relative shear-wave velocity anomaly variation models (Montelli et al., 2006; Ritsema et al., 2011; Auer et al., 2014; French and Romanowicz, 2015) at about 660 km depth (a., c., e. and g.), and at about 2800 km depth (b., d., f. and h.). Black triangle symbolises hotspot present location, according to our positioning (Table 1). EA – East-Africa; LV – Lake-Victoria.

location. The computed coordinates (6°N, 34°E) correspond to a classified hotspot, namely the East-Africa hotspot (Mantle Plumes, 2017 website, see references).

(3) The Lake-Victoria hotspot's current position was determined from tomographic studies to be 3°S, 38°E (Montelli et al., 2006; Ritsema et al., 2011; French and Romanowicz, 2015).

We have used and compared different global tomographic models (Montelli et al., 2006; Ritsema et al., 2011; Auer et al., 2014; French and Romanowicz, 2015) in order to highlight hotspot features in the mantle (Fig. 1). In local tomographic models, the three studied hotspots are located in a broad low-velocity area and can be shown in the upper mantle (see also Sicilia et al., 2008; Hansen et al., 2012). At about 660 km depth, the Afar and Lake-Victoria hotspots are located in low-velocity shear-wave regions in each model (Figs. 1.a, 1.c, 1.e and 1.g). At the same depth, the East-Africa hotspot seems located at the edge of low-velocity shear-wave regions (Figs. 1.a, 1.e and 1.g), with the exception of the S4ORTS model (Fig. 1.c) where the East-Africa hotspot is situated in a low-velocity area, alike the two other hotspots. According to the four tomographic models (Figs. 1.b, 1.d, 1.f and 1.h) the Lake-Victoria and East-Africa hotspots are located at the edge of a low-velocity area at deeper depth (2800 km). This is not the case for the Afar hotspot, never frankly associated to any low velocity area. As claimed by Davaille et al. (2005) the Afar hotspot does not display a strong clear anomaly at the base of the mantle. Thus, tomographic images suggest that the three plumes are rooted at least down to about 660 km depth (Fig. 1). The lack of a clear tomographic signature in the upper mantle for the East-Africa hotspot may be related to the existence of a huge volcanic eruption leading to the eruption of the Ethiopian–Yemen traps at 32 Ma (Hofmann et al., 1997), such that its plume conduit may no longer be fed by volcanic material up to the present day.

2.3. Hotspot reference frame comparison

We compared several hotspot reference frames in order to select the one that best fit the hotspot tracks with their expected consequences, according to a selected plate circuit (Table A1, Appendix A).

Müller et al. (1993), O'Neill et al. (2005), Torsvik et al. (2008) and Doubrovine et al. (2012) published four different hotspot reference frames, from 120 Ma to the present. Two different philosophies were used. The first one is called the 'fixed hotspot' model. It is assumed that (1) present day hotspots are the surface expression of a mantle plume, anchored to the core-mantle boundary, and (2) these plumes remain reasonably fixed with respect to one another, the hotspot motion being an order of magnitude slower than the plate motion (see Morgan, 1981; Müller et al., 1993). Alternatively, the 'moving hotspot' model (Steinberger and O'Connell, 2000; O'Neill et al., 2005) assumes that hotspot upwelling is perturbed by mantle convection, and that its trajectory must be corrected using a mantle flow model. However, this method is subject to caution, since thermal diffusion is known to preclude predictions older than 75 Ma (Conrad and Gurnis, 2003). Plume motion is derived from an initial vertical conduit, which is advected thanks to a global flow field, as derived from present day mantle.

Müller et al. (1993) elaborated a fixed hotspot reference frame back to 130 Ma by adjusting the dated hotspot tracks of five plates relative to present day hotspot locations. The three other reference frames used backwards advection mantle flow models to compute hotspot motion. O'Neill et al. (2005) improved the model of Müller et al. (1993) by using a modified Hellinger criterion (Hellinger, 1981), in order to match hotspots with volcanic seamounts back to 120 Ma, and also a plume motion model, based on Steinberger and O'Connell's (2000) advecting model. The Hellinger criterion consists of finding the rotation of a plate by reconstructing conjugate fracture zones and isochron segments, such that each of these el-

ements are described as a great circle segment (Hellinger, 1981). O'Neill et al. (2005) modified this criterion by substituting, respectively, fracture zone and isochron segment by hotspot track and dated volcanic seamount. Torsvik et al. (2008) built a global moving hotspot reference frame, based on their own plate circuit and seafloor volcanic ridges. Between the present day and 83.5 Ma, they defined three time-ranges with a constant rotation rate of the African plate. These time-ranges are based on four hotspot tracks, linked to the Hawaii, Louisville, Réunion and Tristan da Cunha hotspot activities, which are characterised by a change in direction of volcanic ridges that occurred during the same time-interval. Torsvik et al. (2008) made a sum between their computed Euler poles at $t = 83.5$ Ma and the stage poles defined by Müller et al. (1993), in order to derive a model going back to 130 Ma. Doubrovine et al. (2012) defined a moving hotspot reference frame using both Indo-Atlantic and Pacific tracks, with a refined plate circuit model linking the Pacific plate with the Indian Ocean bordering continents.

We then compared the predicted tracks of the Tristan da Cunha, Réunion, Kerguelen and East-Africa hotspots for each of the four models with the observed hotspot tracks of the Walvis, Chagos-Laccadive and Mascarene-Seychelles ridges (Fig. 2). We also represented, for each model, the expected hotspot trajectories for the Lake-Victoria and Afar hotspots (Fig. B1, Appendix B).

We observed that the predicted hotspot tracks of Müller et al. (1993) and O'Neill et al. (2005), for the Tristan da Cunha and Réunion hotspots, fit well with the Walvis, Chagos-Laccadive and Mascarene-Seychelles ridges. The Kerguelen hotspot track in both models is also situated close to the Ninetyeast Ridge, at a distance of about 500 km east (Figs. 2.a, 2.b). The hotspot tracks predicted by the global moving hotspot reference frame of Torsvik et al. (2008) are not as closely correlated with the ridges (Fig. 2c) – the Tristan da Cunha track is quite well superimposed on the Walvis Ridge, but the Kerguelen track is significantly shifted (by about 800 km) east of the Ninetyeast Ridge. Finally, the model of Doubrovine et al. (2012) displays large discrepancies between the volcanic seamount ridges and the hotspot tracks (Fig. 2d), the derived Tristan da Cunha track being shifted southeast of the Walvis Ridge for times earlier than 60 Ma, and the Kerguelen track being shifted about 1000 km east of the Ninetyeast Ridge.

From a published database of dated volcanic edifices along ridges (see Table C1, Appendix C), we computed the distance between each expected hotspot location and the dated volcanic seamounts for the four compared hotspot reference frames (Fig. 3):

(1) The East-Africa hotspot track derived from the model of O'Neill et al. (2005) better correlates hotspot expected location and dated volcanism (Fig. 3.a);

(2) The calculated distance between derived hotspot location and dated oceanic volcanism along the Kerguelen hotspot track are, for the four hotspot reference frames, greater than 400 km. However, the reference frame of O'Neill et al. (2005) gives better results at 57.9 Ma, 60.9 Ma, 81.8 Ma and 118.2 Ma (Fig. 3.b);

(3) The Réunion track is not discriminant, all reference frames being equivalent (Fig. 3.c);

(4) The hotspot locations derived from the reference frame of Müller et al. (1993) are in good agreement with dated volcanism in the case of the Tristan da Cunha track (Fig. 3.d).

From these two comparative methods (qualitative in Fig. 2, and then quantitative in Fig. 3), it appears that the hotspot models of Müller et al. (1993) and O'Neill et al. (2005) better associate hotspot past location with the observed chain of volcanic seamounts. The oceanic ridges are not well predicted by the Tristan da Cunha or even the Kerguelen hotspot tracks in the two other models. Therefore, we selected the reference frame of O'Neill et al. (2005) for our reconstructions, the distances between dated oceanic seamounts of the Ninetyeast Ridge and past Kerguelen

hotspot locations being more reasonable than those of the others (Fig. 3.b) and, even for the most ancient parts of these paths, better than the model of Müller et al. (1993). Moreover, we chose to use their non-interpolated Euler pole at 110 Ma, because of a better correspondence between continental volcanism and the past expected hotspot location (see Fig. 2.b).

2.4. Hotspot tracks back to 110 Ma

We computed the hotspot trajectories from the present day to 110 Ma, using the O'Neill et al. (2005) hotspot reference frame (Table A1, Appendix A) and assuming that hotspots are fixed and stable features over time in the mantle (Davaille et al., 2005), such that hotspot consequences should be observable from the vertical of the hotspot locations. We used 10 Myr time-interval Euler poles, and considered O'Neill et al.'s (2005) interpolated poles at 20 Ma, 70 Ma and 80 Ma. The hotspot track was computed with respect to the plate (Arabia or Africa) under which it was located at the considered time (Fig. 4). The Afar hotspot is attached to Africa from the present to 5 Ma, the East-Africa hotspot from the present to 90 Ma, and the Lake-Victoria hotspot from the present to 94 Ma. Hotspot locations were transferred to the Arabian plate, according to Red Sea opening parameters. Our motion between Arabia and Africa is from Le Pichon and Gaulier (1988), their study being based on several datasets (magnetic anomalies in the Gulf of Aden and northern Red Sea and geological constraints quantifying the motion along the Levant Fault Zone and the Gulf of Suez). Only an insignificant misfit of $\sim 1\text{--}2^\circ$ was found by using the parameters of Fournier et al. (2010).

The Afar hotspot expected track goes from northeast of Arabia, continuing along the eastern boundary of the plate, close to the present Zagros Front (Fig. 4). At 50 Ma, it bifurcated towards the present Afar triple junction, where it is located at the moment (Fig. 4). The East-Africa expected hotspot path exactly followed the incipient plate boundary between Africa and Arabia, i.e., the present Red Sea, from 90 Ma to 40 Ma. At 40 Ma, it was below the site of the present Afar triple junction, and continued its travels to its present location (Fig. 4). The Lake-Victoria hotspot went from the middle part of the present Red Sea and travelled southward to its current location (Fig. 4).

3. Evidence of hotspot activity along their predicted tracks

Evidence of hotspot activity was then searched for, along their predicted paths. We particularly focused on: (1) heat-flow anomalies caused by hotspot heating; (2) uplift due to plume buoyancy [dependent on the plume head temperature and how close the top of the plume was to the base of the crust (Campbell, 2001)]; and (3) geochemical signatures of alkali basalt volcanism, indicating a plume origin [i.e. enriched in light rare earth elements and/or incompatible elements (Campbell, 2001)]. We supposed that any hotspot effects would be seen within a circle of 500 km diameter at the surface, keeping in mind that this area could be wider if the plume head had spread under the continental lithosphere. We also assumed that all hotspot effects occurred above the hotspot's expected location, according to the comparison of O'Neill et al. (2005), between the fixed and moving hotspot reference frame. We considered the advection of plumes to be of minor significance.

3.1. Lake-Victoria hotspot track

Cenozoic volcanism is known from along the Lake-Victoria hotspot predicted trajectory (Fig. 4). This volcanism does not follow exactly the Lake-Victoria hotspot path, but is located on the Kenyan rift, some 500 km to the west. Alkaline to basic lavas (Pik et al., 2006) were extruded in the Eocene (i.e., before rifting) in

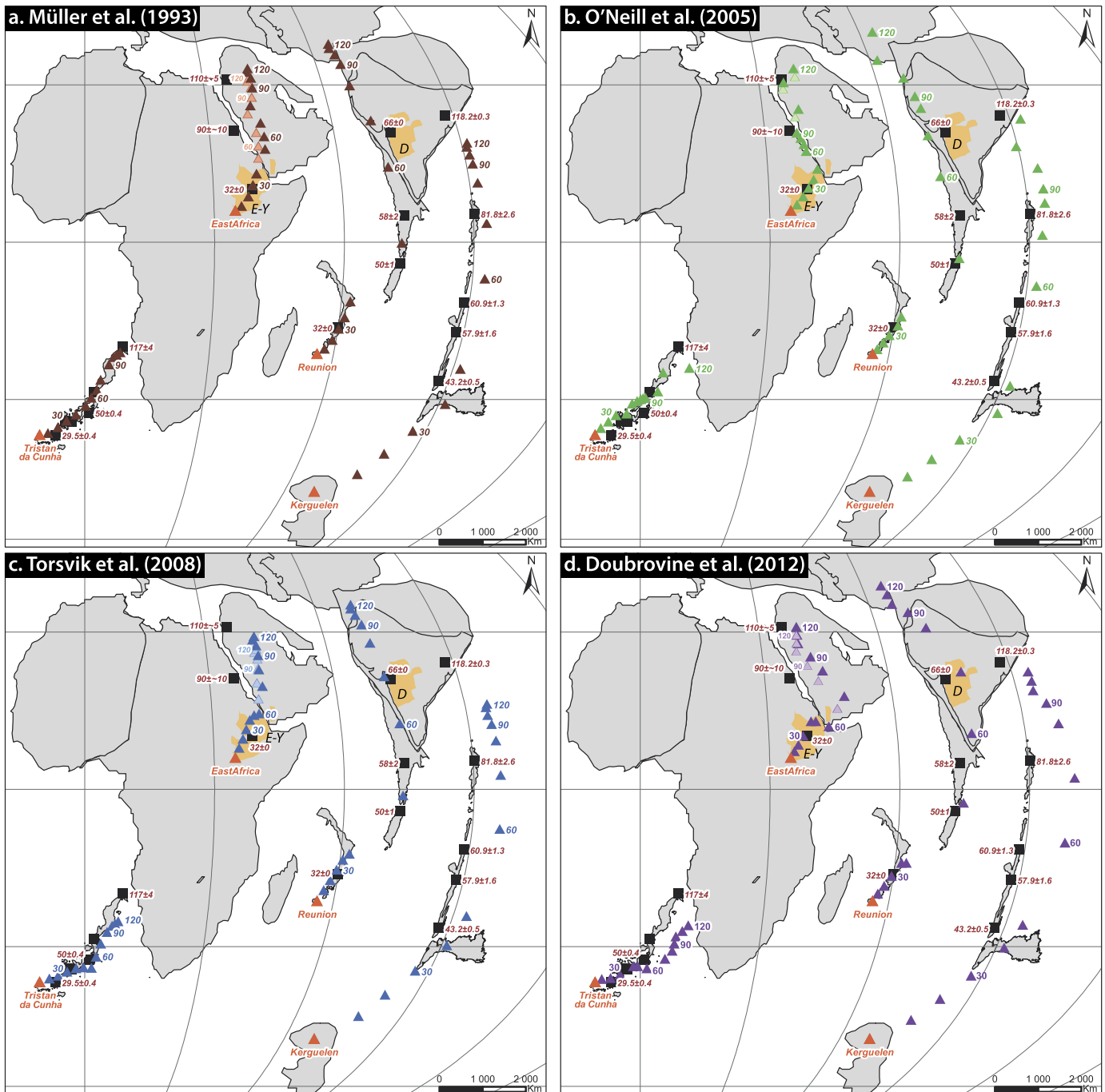


Fig. 2. Comparison between four hotspot reference frames: (a.) the fixed hotspot reference frame of Müller et al. (1993); (b.) the moving hotspot reference frame of O'Neill et al. (2005); (c.) the global moving hotspot reference frame of Torsvik et al. (2008); and (d.) the moving hotspot frame of Doubrovine et al. (2012). Orange triangle – present day hotspot location. Triangle – hotspot track on each frame with a timescale interval plot of 10 Myr. Light triangles for the East-African hotspot path are derived according to the African plate, such that we do not consider the opening of the Red Sea and the Gulf of Aden. Black square – dated volcanism (see Table C1, Appendix C for the age references). D – Deccan traps. E-Y – Ethiopian–Yemen traps.

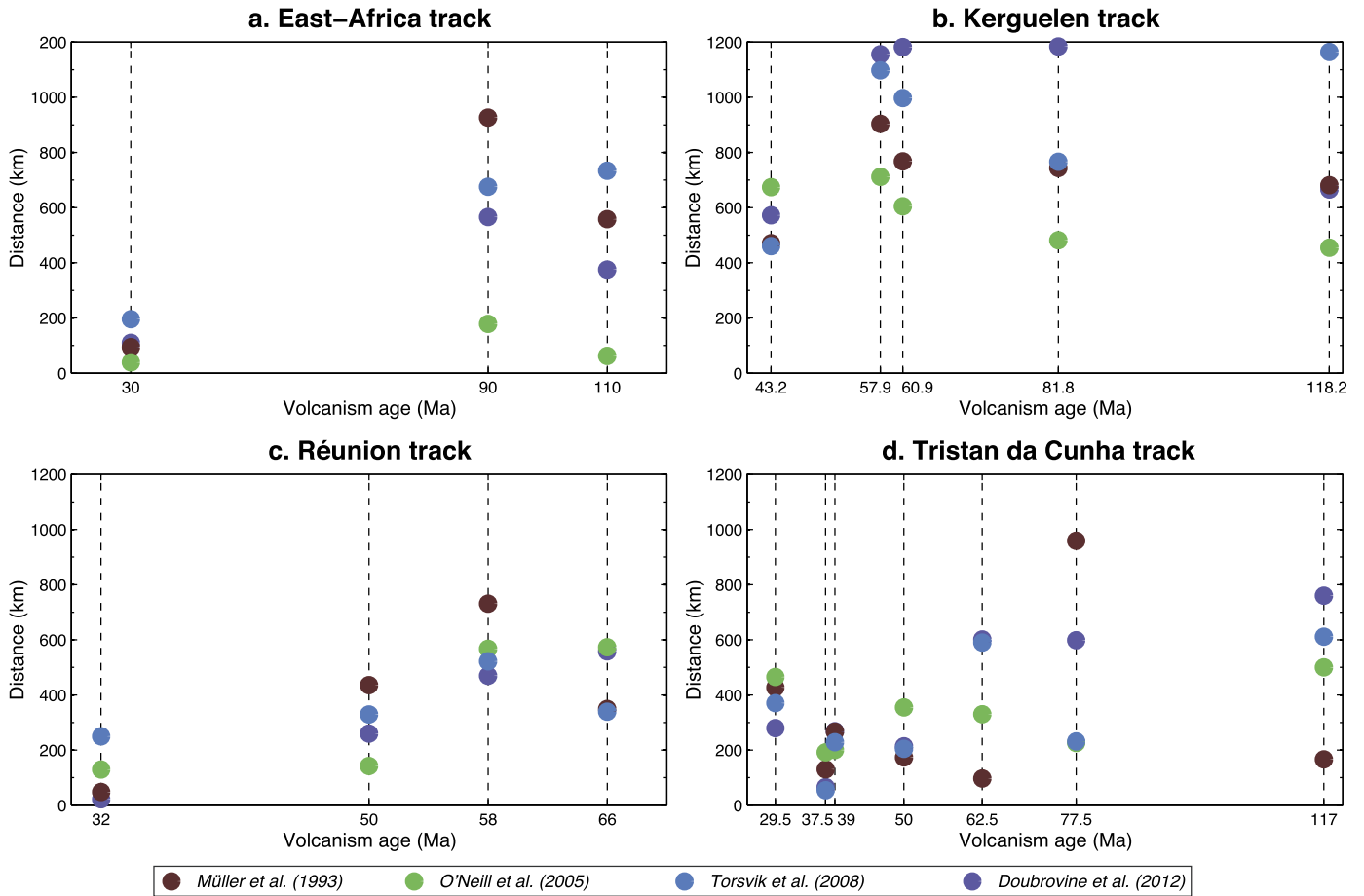


Fig. 3. Distance plots between the relative dated volcanism and the past expected hotspot location in each reference frame for the East-Africa (a.), Kerguelen (b.), Réunion (c.) and Tristan da Cunha (d.) hotspot tracks, respectively.

the Kenya Rift region, and propagated southwards through Kenya, reaching northern Tanzania during the Late Miocene (MacDonald et al., 2001). This volcanism has a mantle plume isotopic signature (Pik et al., 2006; Halldórsson et al., 2014), and the area surrounding the Lake-Victoria hotspot's present location is characterised by a long-wavelength dome (Fig. 4) (Ebinger et al., 1989; Koptev et al., 2015).

3.2. Afar hotspot track

Afar hotspot activity is marked by recent volcanic activity, the 4 Ma Stratoid Series (see a review in Stab et al., 2016) (Fig. 4). The present day hotspot location (Fig. 4) is located in a long-wavelength dome (Ebinger et al., 1989). No volcanism or uplift have been observed along the Afar path back to 110 Ma. We searched for a possible thermal anomaly, caused by past hotspot heating. We performed a heat-flow study on the Arabian plate, using temperature data from 399 boreholes, complemented by 123 other heat-flow data (Morgan et al., 1985; Rolandone et al., 2013) (Fig. 5.a). We estimated the heat-flow for each borehole, according to Fourier's law (Fig. 5.a). The thermal gradient was calculated and the thermal conductivity estimated, using the sedimentary cover lithology, and assuming that it remained relatively constant over Arabia. A mean value of 3 W/m/K was set. If we consider instantaneous heating due to a hotspot, we can estimate the heat diffusion time (τ), according to the following equation (Turcotte and Schubert, 2014):

$$\tau = \frac{z_l^2 \rho C_p}{2.322^2 k},$$

where z_l is the thickness of the lithosphere, k the thermal conductivity (3 W/m/K), ρ the density (2700 kg m^{-3}) and C_p the thermal heat capacity (1000 J/kg/K). The mean Arabian plate thickness is about 150 km. We decided to use this present day value in order to estimate how long the thermal anomaly would be dissipated, as we could not determine precisely the thickness of the lithosphere before the hotspot impact. Thus, for a lithospheric thickness of 50, 100, 150 and 200 km, we derive respectively a heat diffusion time of ~ 14 , ~ 55 , ~ 125 and ~ 223 Myrs. For the Arabian plate, the computed heat diffusion time of ~ 125 Myr suggests that it is possible to keep the memory of a hotspot thermal anomaly. We noted that, if the plate is thin (50 km), then a thermal anomaly is rapidly dissipated. However, for a plate thickness of at least 100 km, the derived heat diffusion time is long enough to suggest the possibility of measuring a thermal anomaly in present day heat-flow data.

In order to find a continental heat-flow anomaly linked to a hotspot, we only used data located far away from ridge zones, in order to avoid interference with the Red Sea or the Gulf of Aden. Thus, we examined a heat-flow transect, combined with its respective elevation and lithospheric thickness profiles (Globig et al., 2016) (Fig. 5.b). The thickness model of Globig et al. (2016) was derived from a combined model of elevation and geoid anomaly, subsequently coupled with a thermal analysis. To ensure the validity of their model estimates of the lithosphere-asthenosphere boundary, tomographic models, elevation and geoid data were used for testing.

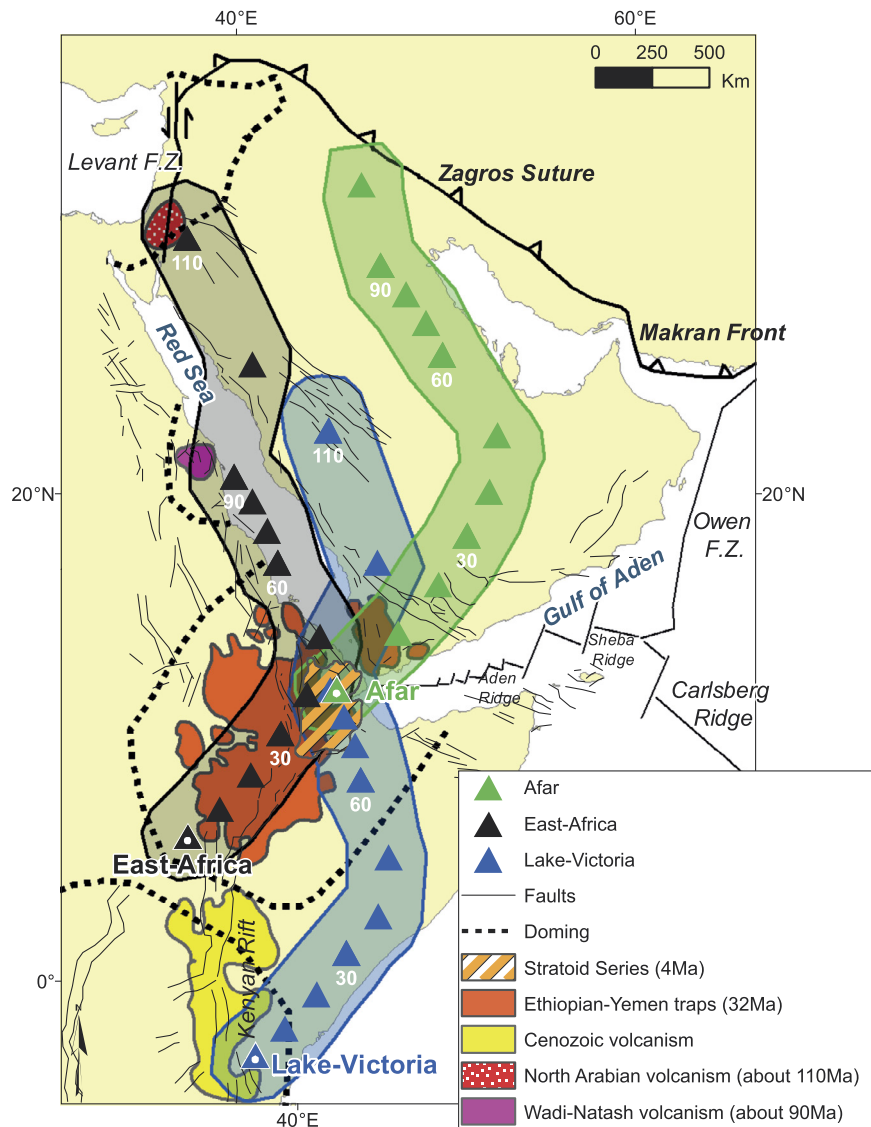


Fig. 4. Geological context of the Arabian and African plates. The computed hotspot tracks were determined with a 10 Myr time-interval, according to O'Neill et al. (2005). Triangles with white dots – present day hotspot coordinates. Shaded area – minimum influence area of a hotspot with a diameter of 500 km. Note that the Ethiopian–Yemen traps are situated at the junction of the East-Africa and Lake-Victoria hotspot paths. Map presented as a Robinson projection.

The profile ABB' crosses the Afar path at ~ 45 Ma (Fig. 5.a). We observed a high heat-flow value on the Red Sea (≥ 150 mW/m²), explained by the seafloor spreading geodynamic context, a low heat-flow in the Arabian Shield (≤ 50 mW/m²), and a high heat-flow value (about 100 mW/m²) located along the supposed past location of the Afar track (Fig. 5.b). If we suppose no heat-flow interference, due to the Red Sea and the Gulf of Aden seafloor spreading and according to the thickness of the lithosphere, we can assume that the high heat-flow observed on the eastern part of the Arabian plate corresponds to the Afar hotspot thermal memory. The absence of interference with the Red Sea and Gulf of Aden seems reasonable, because heat-flow values determined on the edge of the Arabian plate, close to the Gulf of Aden, are very low, compared to those measured in the Gulf of Aden (Fig. 5.a). It is not possible to find hotspot track evidence before 90 Ma due to the Zagros Mountains. Thus, our data only suggest a track back to 90 Ma.

3.3. East-Africa hotspot track

The East-Africa hotspot track is highlighted in three areas by volcanic activity, coupled with regional uplift (Fig. 4).

At 110 Ma, the East-Africa hotspot was located under the Levant. At that time, this area was the site of intrusive alkaline volcanism, which lasted from the Neocomian until the Cenomanian, combined with a several-hundred-kilometre-wide uplift. This Early Cretaceous uplift extended from Lebanon and central Syria to the Sinai (Fig. 4) (Garfunkel, 1998; Gvirtzman et al., 1998). The uplift is demonstrated thanks to geological analysis, highlighting a hiatus of Jurassic and Triassic deposits. This hiatus is interpreted as resulting from a huge erosion episode related to major uplift, associated with volcanism during the Lower Cretaceous, up to Aptian times (Gvirtzman et al., 1998). The paleogeographic review of Ziegler (2001), at the scale of Arabia, is in agreement with this interpretation, showing also an emersion of the area concerned during the Lower Cretaceous. In addition, and according to basalt isotopic composition, a mantle plume origin is proposed (Stein and Hofmann, 1992). Thus, these two related phenomena (uplift and volcanism) are likely associated with hotspot activity.

At 90 Ma, the East-Africa hotspot track was underscored by the Wadi-Natash volcanic area (Fig. 4). In this area, two phenomena could be due to hotspot activity – the Wadi-Natash alkaline basalt, dated at about 90 Ma, and a coeval regional uplift, as indi-

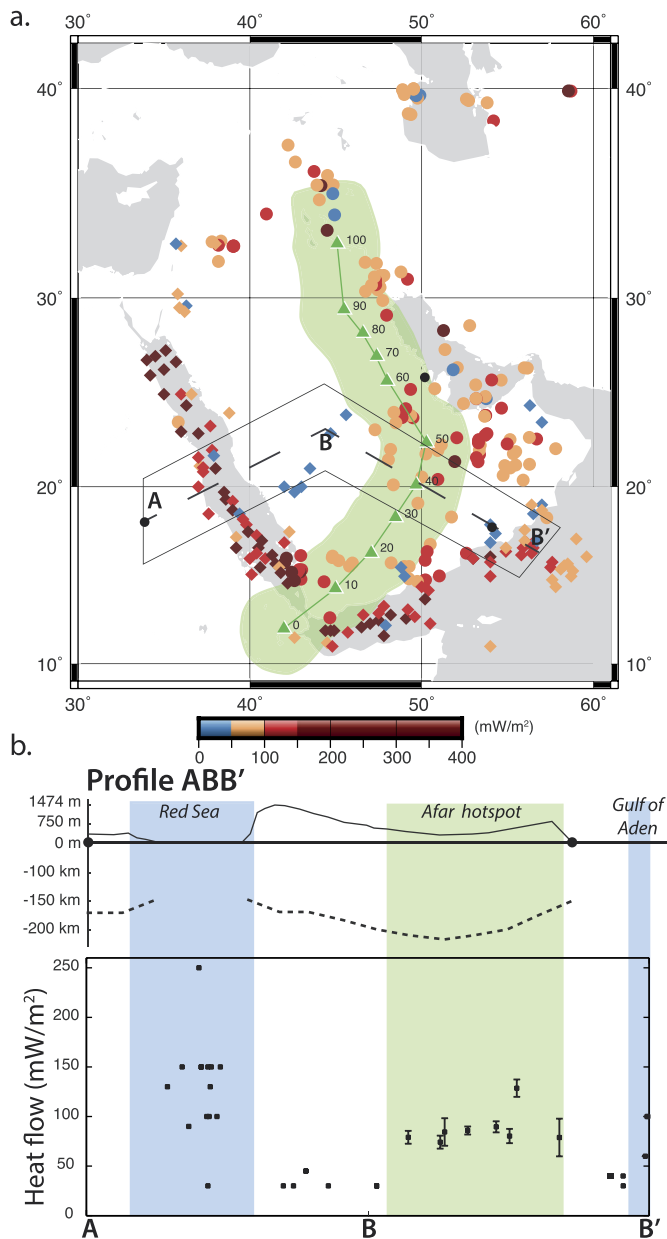


Fig. 5. (a.) Map of Arabian plate heat-flow. Diamonds – heat-flow data from Morgan et al. (1985) and Rolandone et al. (2013). Dots – heat-flow data estimated from borehole data (TOTAL database). Green triangles symbolise the Afar hotspot location over time, according to the O'Neill et al. (2005) hotspot reference frame. The green shaded area embodies the minimum hotspot influence area, where hotspot consequences should be found. (b.) Heat-flow profile along ABB', which crosses the Afar hotspot path at ~45 Ma. The blue shaded area embodies high heat-flow values linked to the geological context. Only data with an error of less than 20 mW/m² are plotted. The heat-flow map is presented as a cylindrical projection. Corresponding topographic profiles relative to the sea floor (solid line), and the thickness of the lithosphere (dashed line) were determined with Google Earth software and the lithospheric model of Globig et al. (2016), respectively.

cated in the literature (Ressetar et al., 1981; Crawford et al., 1984; Hubbard et al., 1987; Mohamed, 2001). Between 40 Ma and 30 Ma, the East-Africa hotspot was located under the Ethiopian–Yemen traps, which set up at 32 Ma. Isotopic studies performed on these traps suggest a deep plume origin (Halldórsson et al., 2014). Moreover, a large-scale dome, related to a mantle plume, exists and extends into the traps area (Ebinger et al., 1989). We noted that the Ethiopian–Yemen traps occurred at the East-Africa and Lake-Victoria hotspot junction.

Isotopic studies performed on Red Sea glass samples from the Red Sea axis exemplify an isotopic composition suggesting a mantle plume contamination (Moreira et al., 1996; Pik et al., 2006; Halldórsson et al., 2014). Although the helium isotopic ratio in samples from north of the Red Sea (e.g., Mabahiss Deep) shows a similar value to the mean mid-ocean ridge basalt (MORB) value (Moreira et al., 1996), neon isotopes contrarily suggest that a primitive material (plume-like) may be present in the north of the Red Sea. Indeed, using the data from Red Sea basalts from Moreira et al. (1996), we can correct the measured $^{21}\text{Ne}/^{22}\text{Ne}$ isotopic ratios for the atmospheric neon using the method of Moreira and Allègre (1998), and a mantle $^{20}\text{Ne}/^{22}\text{Ne}$ ratio of 12.6. These corrected for air ($^{21}\text{Ne}/^{22}\text{Ne}$)_c ratios show values as low as 0.044 ± 0.004 in the northern part of the Red Sea, significantly lower than the MORB value of 0.060 (Moreira et al., 1998). This suggests that a primitive reservoir (in terms of noble gases), having a low $^{21}\text{Ne}/^{22}\text{Ne}$ ratio, was sampled by basalts from the northern part of the Red Sea. The fact that neon is able to detect this primitive reservoir, whereas helium clearly does not, is due to the different $^3\text{He}/^{22}\text{Ne}$ ratios of the two reservoirs (MORB and primitive), making neon a better proxy for plume detection than helium, as discussed by Moreira et al. (1998) and Tucker and Mukhopadhyay (2014).

4. Discussion

The discrepancy between oceanic and continental lithosphere, in terms of hotspot volcanism, is explained by their respective thicknesses – the thicker the lithosphere, the less surface volcanism is observed (Davies, 1994; Davies et al., 2015). Consequently, the number of continental volcanic occurrences can be explained by the lithosphere thickness, about 180 km in the region, compared to the approximately 140 km lithosphere thickness of the region where volcanic traps are well expressed (Globig et al., 2016).

It is possible to identify hotspot activity along the three predicted tracks, using heat-flow data, occurrences of volcanism, mantle plume isotopic signatures and uplift. The East-Africa hotspot seems to be the most active, as three identified volcanic episodes occurred along its trajectory. The two main volcanic episodes are the Ethiopian–Yemen traps and the Stratoid Series, which are separated by a quiescent phase of 28 Myr (Stab et al., 2016). Our analysis demonstrates that the Afar hotspot could not have been the trigger of the Ethiopian–Yemen traps (Steinberger, 2000; Courtillot et al., 2003; Bosworth et al., 2005) because it was located 1,000 km away from them, whichever hotspot reference frame is used. By contrast, the East-Africa hotspot was just at the right position (Fig. 4). Consequently, we suggest that the East-Africa hotspot is the main contributor to the Ethiopian–Yemen traps. The Afar hotspot, well imaged by tomographic studies down to at least 1,000 km (Montelli et al., 2006; French and Romanowicz, 2015), is most probably at the origin of the Stratoid Series (Fig. 4).

Based on tomographic studies (Fig. 1), the Afar and Lake-Victoria hotspots were imaged down to at least the transition zone, while the East-Africa hotspot has no clear signature in the upper mantle (Debaille et al., 2001; Montelli et al., 2006; French and Romanowicz, 2015). Instead of being anchored deep at the core-mantle boundary, the three hotspots could equally have originated from a primary plume (Fig. 6), linked to the African superswell (Davaille et al., 2005; Civiero et al., 2015; French and Romanowicz, 2015), giving rise to three secondary plumes. Our study supports this interpretation. According to an analogue model plume lifetime, it is possible that a plume, rising up from 2800 km depth, can remain at the transition zone, as long as its thermal buoyancy is high enough (Davaille et al., 2005). If the original plume is wider than 1,000 km in diameter, then new secondary plumes could develop, with spacing ranging from 500 km to 1000 km (Kumagai et al., 2007). According to the S receiver

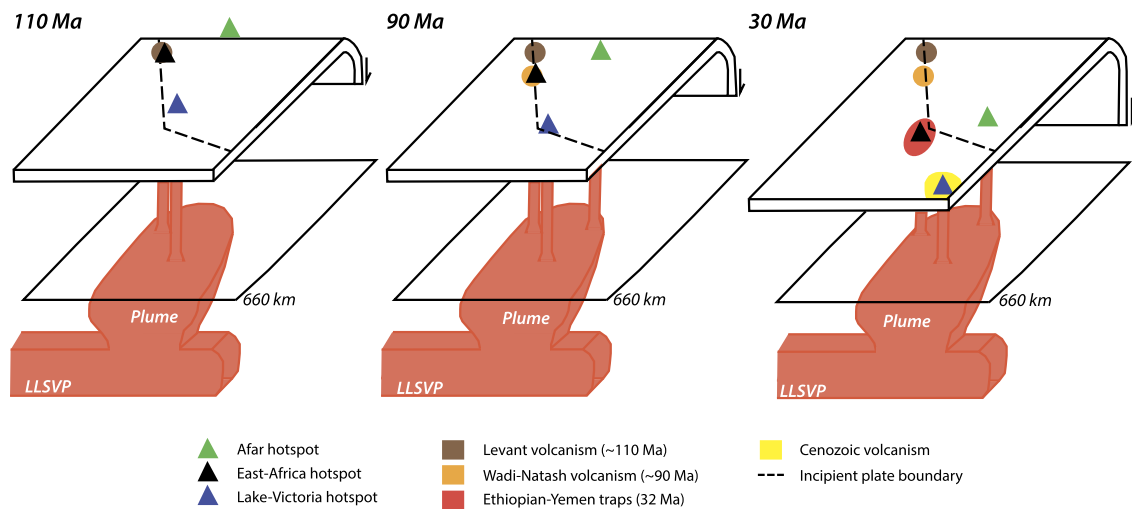


Fig. 6. Scenario illustrating hotspot organisation in the Earth's mantle (not to scale). According to tomographic studies (Debayle et al., 2001; Montelli et al., 2006; French and Romanowicz, 2015), geochemical isotopic signatures (Rogers et al., 2000; Halldórsson et al., 2014) and analogue plume models (Davaille et al., 2005; Kumagai et al., 2007), the three hotspots may have originated from the same plume at least 90 Ma. It is difficult to trace the Afar hotspot before this because the Neo-Tethys subduction zone crosses the track. At 110 Ma, the East-Africa hotspot formed a volcanic area in the Levant zone (Garfunkel, 1998; Gvirtzman et al., 1998), then the Wadi-Natash volcanic complex area at about 90 Ma (Ressetar et al., 1981; Crawford et al., 1984; Hubbard et al., 1987) and, finally, started the Ethiopian–Yemen traps at 32 Ma. The Lake-Victoria hotspot is linked to Cenozoic volcanism (Pik et al., 2006; Halldórsson et al., 2014). Since 30 Ma, no volcanism has been associated with Afar hotspot activity.

function technique, performed beneath Afar and the neighbouring regions, it seems that two separate bodies lie beneath these regions, i.e., the East-Africa and Afar hotspots (Vinnik et al., 2004). Moreover, Debayle et al. (2001) suggested several narrow plume tails under eastern Africa (Fig. 6). Apart from this, geochemical studies argue that at least two different plume heads are located under the Afar region and the Kenya Dome (Rogers et al., 2000; Halldórsson et al., 2014).

The thermal study along the Afar hotspot track shows that the lithosphere records the hotspot path. Thus, all along the East-Africa hotspot track, the lithosphere was likely weakened by its heating (Burov and Gerya, 2014). This weakening was transient and remained until the lithosphere recovered its initial temperature. We note that the present thickness of the lithosphere along the profile ABB' is about 200 km thick (Fig. 4b), while it underwent a hotspot impact at about 45 Ma ago. Nevertheless, according to the studies of Monnereau et al. (1993), the moving lithosphere is not significantly affected by the thermal erosion process even if the plate velocity is slow, while its temperature profile is considerably affected (Davies, 1994).

Separation of the Arabian plate occurred along the Gulf of Aden and the Red Sea, a consequence of plate boundary extensional forces, caused by mantle delamination, associated with the Arabia-Eurasia collision in the Zagros (Hatzfeld and Molnar, 2010). The Gulf of Aden is directly superimposed on a Mesozoic rift system (Autin et al., 2013), and developed between two weak points, the Carlsberg Ridge extremity and the past East-Africa hotspot location (Fig. 4). Then, break-up occurred along the East-Africa hotspot path (Fig. 4), giving birth to the Red Sea and the separation of Arabia and Africa. So, the East-Africa hotspot interfered in two different ways during the separation of the Arabian plate, by: (1) propagating the rupture between it and another weak zone (the moving extremity of the Carlsberg Ridge), and (2) generating thermal weakening of the continental lithosphere along its past trajectory. The existence of a relationship between rift and hotspot has already been well established (Burke and Dewey, 1973; Courtillot et al., 1999). Burov and Gerya (2014) and Frizon de Lamotte et al. (2015) proposed that the role of the hotspot was to localise, rather than to trigger the rift. Our work, emphasising the role of the hotspot trajectory and related thermal memory, complements this point of view, and explains the resulting rift pattern.

5. Conclusions

Using a hotspot reference frame, we computed the continental track location of three present day hotspots – Afar, East-Africa and Lake-Victoria – back to 110 Ma. We then checked for geological evidence of their past activity along their tracks, using dated occurrences of uplift, related volcanism, and/or heat-flow data. The East-Africa and Afar hotspot activities were ascertained, at least episodically, back to 110 Ma and 90 Ma, respectively. No activity of the Lake-Victoria hotspot was evidenced prior to the Cenozoic. The East-Africa hotspot track led to two observations. Firstly, the Afar hotspot cannot be the origin for the Ethiopian–Yemen traps because it was located too far away from the traps at 30 Ma. Through reconstruction, the East-Africa hotspot is a better candidate for explaining this volcanic activity. We noted that the Ethiopian–Yemen traps and the Stratoid Series were established at the junction of the three hotspots. Additionally, the superimposition of the Red Sea axis and the East-Africa hotspot path supports a causal relationship between thermal weakening along the hotspot path trajectory and the subsequent Red Sea rift system location. To go further, a numerical modelling will be done in order to evaluate the consequences of a hotspot impact on the rheological properties of the lithosphere. Finally, the existence of hotspot-related activity along the East-Africa track as far back as the Cretaceous shows that the related plume was possibly episodically active long before the eruption of the Ethiopian–Yemen traps, indicating that continental flood basalts can be related to the evolution of a pre-existing plume, and are not necessarily linked to the birth of a new one.

Acknowledgements

We thank A. Davaille, M. Moreira F. Lucazeau and F. Lopes for their fruitful discussions about hotspots, geochemistry data, heat flow interpretations and models. We acknowledge Nicolas Flament for its critical reading and comments, which were of great help in improving the quality of the manuscript. Figures were realised thanks to the ArcGis and the GMT (Wessel et al., 2013) software. S. Vicente de Gouveia acknowledges TOTAL for a PhD scholarship. The study is IGP contribution 3916.

Appendix. Supplementary material

Supplementary material related to this article can be found online at <https://doi.org/10.1016/j.epsl.2018.01.030>.

References

- Auer, L., Boschi, L., Becker, T.W., Nissen-Meyer, T., Giardini, D., 2014. Savani: a variable resolution whole-mantle model of anisotropic shear velocity variations based on multiple data sets. *J. Geophys. Res., Solid Earth* 119 (4), 3006–3034.
- Autin, J., Bellahsen, N., Leroy, S., Husson, L., Beslier, M.O., d'Acremont, E., 2013. The role of structural inheritance in oblique rifting: insights from analogue models and application to the Gulf of Aden. *Tectonophysics* 607, 51–64.
- Almalki, K.A., Betts, P.G., Ailleres, L., 2014. Episodic sea-floor spreading in the Southern Red Sea. *Tectonophysics* 617, 140–149.
- Bellahsen, N., Faccenna, C., Funicello, F., Daniel, J.M., Jolivet, L., 2003. Why did Arabia separate from Africa? Insights from 3-D laboratory experiments. *Earth Planet. Sci. Lett.* 216 (3), 365–381.
- Bosworth, W., Huchon, P., McClay, K., 2005. The Red Sea and Gulf of Aden basins. *J. Afr. Earth Sci.* 43 (1), 334–378.
- Burov, E., Gerya, T., 2014. Asymmetric three-dimensional topography over mantle plumes. *Nature* 513, 85–89.
- Burke, K., Dewey, J.F., 1973. Plume-generated triple junctions: key indicators in applying plate tectonics to old rocks. *J. Geol.* 81 (4), 406–433.
- Burke, K.C., Wilson, J.T., 1976. Hot spots on the Earth's surface. *Sci. Am.* 235 (2).
- Campbell, I.H., 2001. Identification of Ancient Mantle Plumes. *Special Papers. Geological Society of America*, pp. 5–22.
- Chu, R., Leng, W., Helmberger, D.V., Gurnis, M., 2013. Hidden hotspot track beneath the eastern United States. *Nat. Geosci.* 6 (11), 963–966.
- Civiero, C., et al., 2015. Multiple mantle upwellings in the transition zone beneath the northern East-African Rift system from relative P-wave travel-time tomography. *Geochem. Geophys. Geosyst.* 16, 2949–2968.
- Claoud, V., Bonneville, A., 2001. How many Pacific hotspots are fed by deep-mantle plumes? *Geology* 29 (8), 695–698.
- Conrad, C.P., Gurnis, M., 2003. Seismic tomography, surface uplift, and the breakup of Gondwanaland: integrating mantle convection backwards in time. *Geochem. Geophys. Geosyst.* 4 (3).
- Courtillot, V., Jaupart, C., Manighetti, I., Tapponnier, P., Besse, J., 1999. On causal links between flood basalts and continental breakup. *Earth Planet. Sci. Lett.* 166 (3), 177–195.
- Courtillot, V., Davaille, A., Besse, J., Stock, J., 2003. Three distinct types of hotspots in the Earth's mantle. *Earth Planet. Sci. Lett.* 205 (3), 295–308.
- Crawford, W.A., Coulter, D.H., Hubbard, H.B., 1984. The areal distribution, stratigraphy and major element chemistry of the Wadi Natash volcanic series, Eastern Desert, Egypt. *J. Afr. Earth Sci.* 2 (2), 119–128.
- Crough, S.T., 1983. Hotspot swells. *Annu. Rev. Earth Planet. Sci.* 11 (165).
- Debayle, E., Lèvéque, J.J., Cara, M., 2001. Seismic evidence for a deeply rooted low-velocity anomaly in the upper mantle beneath the northeastern Afro/Arabian continent. *Earth Planet. Sci. Lett.* 193 (3), 423–436.
- Davaille, A., Stutzmann, E., Silveira, G., Besse, J., Courtillot, V., 2005. Convective patterns under the Indo-Atlantic “box”. *Earth Planet. Sci. Lett.* 239 (3), 233–252.
- Davies, G.F., 1994. Thermomechanical erosion of the lithosphere by mantle plumes. *J. Geophys. Res., Solid Earth* 99 (B8), 15709–15722.
- Davies, D.R., Rawlinson, N., Iaffaldano, G., Campbell, I.H., 2015. Lithospheric controls on magma composition along Earth's longest continental hotspot track. *Nature* 525 (7570), 511–514.
- Doubrovine, P.V., Steinberger, B., Torsvik, T.H., 2012. Absolute plate motions in a reference frame defined by moving hot spots in the Pacific, Atlantic, and Indian oceans. *J. Geophys. Res., Solid Earth* 117 (B9).
- Ebinger, C.J., Bechtel, T.D., Forsyth, D.W., Bowin, C.O., 1989. Effective elastic plate thickness beneath the East African and Afar plateaus and dynamic compensation of the uplifts. *J. Geophys. Res., Solid Earth* 94 (B3), 2883–2901.
- Faccenna, C., Becker, T.W., Jolivet, L., Keskin, M., 2013. Mantle convection in the Middle East: reconciling Afar upwelling, Arabia indentation and Aegean trench rollback. *Earth Planet. Sci. Lett.* 375, 254–269.
- Fournier, M., Chamot-Rooke, N., Petit, C., Huchon, P., Al-Kathiri, A., Audin, L., Beslier, M.-O., d'Acremont, E., Fabbri, O., Fleury, J.-M., et al., 2010. Arabia–Somalia plate kinematics, evolution of the Aden–Owen–Carlsberg triple junction, and opening of the Gulf of Aden. *J. Geophys. Res., Solid Earth* 115 (B4).
- French, S.W., Romanowicz, B., 2015. Broad plumes rooted at the base of the Earth's mantle beneath major hotspots. *Nature* 525 (7567), 95–99.
- Fritz, H., Abdelsalam, M., Ali, K.A., Bingen, B., Collins, A.S., Fowler, A.R., Ghebrea, W., Hauzenberger, C.A., Johnson, P.R., Kusky, T.M., Macey, P., Muhongo, S., Stern, R.J., Viola, G., 2013. Orogen styles in the East African Orogen: a review of the Neoproterozoic to Cambrian tectonic evolution. *J. Afr. Earth Sci.* 86, 65–106.
- Frizon de Lamotte, D., Fourdan, B., Leleu, S., Leparmentier, F., Clarens, P., 2015. Style of rifting and the stages of Pangea breakup. *Tectonics* 34 (5), 1009–1029.
- Garfunkel, Z., 1998. Constraints on the origin and history of the Eastern Mediterranean basin. *Tectonophysics* 298 (1), 5–35.
- Globig, J., Fernández, M., Torne, M., Vergés, J., Robert, A., Faccenna, C., 2016. New insights into the crust and lithospheric mantle structure of Africa from elevation, geoid, and thermal analysis. *J. Geophys. Res., Solid Earth* 121 (7), 5389–5424.
- Gvirtzman, Z., Garfunkel, Z., Gvirtzman, G., 1998. Birth and decay of an intracontinental magmatic swell: Early Cretaceous tectonics of southern Israel. *Tectonics* 17 (3), 441–457.
- Halldórsson, S.A., Hilton, D.R., Scarsi, P., Abebe, T., Hopp, J., 2014. A common mantle plume source beneath the entire East African Rift System revealed by coupled helium–neon systematics. *Geophys. Res. Lett.* 41 (7), 2304–2311.
- Hansen, S.E., Nyblade, A.A., Benoit, M.H., 2012. Mantle structure beneath Africa and Arabia from adaptively parameterized P-wave tomography: implications for the origin of Cenozoic Afro-Arabian tectonism. *Earth Planet. Sci. Lett.* 319, 23–34.
- Hatzfeld, D., Molnar, P., 2010. Comparisons of the kinematics and deep structures of the Zagros and Himalaya and of the Iranian and Tibetan plateaus and geodynamic implications. *Rev. Geophys.* 48 (2).
- Hellinger, S.J., 1981. The uncertainties of finite rotations in plate tectonics. *J. Geophys. Res., Solid Earth* 86 (B10), 9312–9318.
- Hofmann, C., Courtillot, V., Feraud, G., Rochette, P., Yirgu, G., Ketefo, E., Pik, R., 1997. Timing of the Ethiopian flood basalt event and implications for plume birth and global change. *Nature* 389 (6653), 838–841.
- Hubbard, H.B., Wood, L.F., Rogers, J.J., 1987. Possible hydration anomaly in the upper mantle prior to Red Sea rifting: evidence from petrologic modeling of the Wadi Natash alkali basalt sequence of eastern Egypt. *Geol. Soc. Am. Bull.* 98 (1), 92–98.
- Koptev, A., Calais, E., Burov, E., Leroy, S., Gerya, T., 2015. Dual continental rift systems generated by plume–lithosphere interaction. *Nat. Geosci.* 8 (5), 388–392.
- Kumagai, I., Davaille, A., Kurita, K., 2007. On the fate of thermally buoyant mantle plumes at density interfaces. *Earth Planet. Sci. Lett.* 254 (1), 180–193.
- Le Pichon, X., Gaulier, J.-M., 1988. The rotation of Arabia and the Levant fault system. *Tectonophysics* 153 (1–4), 271–294.
- Leroy, S., et al., 2012. From rifting to oceanic spreading in the Gulf of Aden: a synthesis. *Arab. J. Geosci.* 5 (5), 859–901.
- MacDonald, R., Rogers, N.W., Fitton, J.G., Black, S., Smith, M., 2001. Plume–lithosphere interactions in the generation of the basalts of the Kenya Rift, East Africa. *J. Petrol.* 42 (5), 877–900.
- Mohamed, F.H., 2001. The Natash alkaline volcanic field, Egypt: geochemical and mineralogical inferences on the evolution of a basalt to rhyolite eruptive suite. *J. Volcanol. Geotherm. Res.* 105 (4), 291–322.
- Monnereau, M., Rabinowicz, M., Arquis, E., 1993. Mechanical erosion and reheating of the lithosphere: a numerical model for hotspot swells. *J. Geophys. Res., Solid Earth* 98 (B1), 809–823.
- Montelli, R., Nolet, G., Dahlen, F.A., Masters, G., 2006. A catalogue of deep mantle plumes: new results from finite-frequency tomography. *Geochem. Geophys. Geosyst.* 7 (11).
- Moreira, M., Valbracht, P.J., Staudacher, T., Allègre, C.J., 1996. Rare gas systematics in Red Sea ridge basalts. *Geophys. Res. Lett.* 23 (18), 2453–2456.
- Moreira, M., Allègre, C.J., 1998. Helium–neon systematics and the structure of the mantle. *Chem. Geol.* 147, 53–59.
- Moreira, M., Kunz, J., Allègre, C.J., 1998. Rare gas systematics on popping rock: estimates of isotopic and elemental compositions in the upper mantle. *Science* 279, 1178–1181.
- Morgan, W.J., 1981. Hotspot tracks and the opening of the Atlantic and Indian Oceans. In: *The Oceanic Lithosphere*, vol. 7, pp. 443–487.
- Morgan, P., Boulos, F.K., Hennin, S.F., El-Sherif, A.A., El-Sayed, A.A., Basta, N.Z., Melek, Y.S., 1985. Heat flow in eastern Egypt: the thermal signature of a continental breakup. *J. Geodyn.* 4 (1), 107–131.
- Müller, R.D., Royer, J.Y., Lawver, L.A., 1993. Revised plate motions relative to the hotspots from combined Atlantic and Indian Ocean hotspot tracks. *Geology* 21 (3), 275–278.
- Olson, P., Schubert, G., Anderson, C., Goldman, P., 1988. Plume formation and lithosphere erosion: a comparison of laboratory and numerical experiments. *J. Geophys. Res., Solid Earth* 93 (B12), 15065–15084.
- O'Neill, C., Müller, D., Steinberger, B., 2005. On the uncertainties in hot spot reconstructions and the significance of moving hot spot reference frames. *Geochem. Geophys. Geosyst.* 6 (4), Q04003.
- Pik, R., Marty, B., Hilton, D.R., 2006. How many mantle plumes in Africa? The geochemical point of view. *Chem. Geol.* 226 (3), 100–114.
- Ressetar, R., Nairn, A.E.M., Monrad, J.R., 1981. Two phases of Cretaceous-Tertiary magmatism in the eastern desert of Egypt: paleomagnetic, chemical and K–Ar evidence. *Tectonophysics* 73 (1), 169–193.
- Richards, M.A., Hager, B.H., Sleep, N.H., 1988. Dynamically supported geoid highs over hotspots: observation and theory. *J. Geophys. Res., Solid Earth* 93 (B7), 7690–7708.
- Ritsema, J., Deuss, A., Van Heijst, H.J., Woodhouse, J.H., 2011. S40RTS: a degree–40 shear-velocity model for the mantle from new Rayleigh wave dispersion, teleseismic traveltimes and normal-mode splitting function measurements. *Geophys. J. Int.* 184 (3), 1223–1236.
- Rogers, N., Macdonald, R., Fitton, J.G., George, R., Smith, M., Barreiro, B., 2000. Two mantle plumes beneath the East African rift system: Sr, Nd and Pb isotope evidence from Kenya Rift basalts. *Earth Planet. Sci. Lett.* 176 (3), 387–400.

- Rolandone, F., Lucazeau, F., Leroy, S., Mareschal, J.C., Jorand, R., Goutorbe, B., Bouquerel, H., 2013. New heat flow measurements in Oman and the thermal state of the Arabian Shield and Platform. *Tectonophysics* 589, 77–89.
- Sicilia, D., Montagner, J.P., Cara, M., Stutzmann, E., Debayle, E., L epine, J.C., L ev eque, J.-J., Beucler, E., Sebai, A., Roult, G., Ayele, A., Sholan, J.M., 2008. Upper mantle structure of shear-waves velocities and stratification of anisotropy in the Afar Hotspot region. *Tectonophysics* 462 (1), 164–177.
- Stab, M., Bellahsen, N., Pik, R., Quidelleur, X., Ayalew, D., Leroy, S., 2016. Modes of rifting in magma-rich settings: tectono-magmatic evolution of Central Afar. *Tectonics* 35, 2–38.
- Stein, M., Hofmann, A.W., 1992. Fossil plume head beneath the Arabian lithosphere? *Earth Planet. Sci. Lett.* 114 (1), 193–209.
- Steinberger, B., 2000. Plumes in a convecting mantle: models and observations for individual hotspots. *J. Geophys. Res., Solid Earth* 105 (B5), 11127–11152.
- Steinberger, B., O'Connell, R.J., 2000. Effects of mantle flow on hotspot motion. In: *The History and Dynamics of Global Plate Motions*, pp. 377–398.
- Thiessen, R., Burke, K., Kidd, W.S.F., 1979. African hotspots and their relation to the underlying mantle. *Geology* 7 (5), 263–266.
- Torsvik, T.H., M uller, R.D., Van der Voo, R., Steinberger, B., Gaina, C., 2008. Global plate motion frames: toward a unified model. *Rev. Geophys.* 46 (3).
- Tucker, J.M., Mukhopadhyay, S., 2014. Evidence for multiple magma ocean outgassing and atmospheric loss episodes from mantle noble gases. *Earth Planet. Sci. Lett.* 393, 254–265.
- Turcotte, D.L., Schubert, G., 2014. *Geodynamics*. Cambridge University Press, pp. 276–282.
- Vinnik, L.P., Farra, V., Kind, R., 2004. Deep structure of the Afro-Arabian hotspot by S receiver functions. *Geophys. Res. Lett.* 31 (11).
- Wessel, P., Smith, W.H.F., Scharroo, R., Luis, J.F., Wobbe, F., 2013. Generic mapping tools: improved version released. *Eos Trans. AGU* 94, 409–410.
- Ziegler, M.A., 2001. Late Permian to Holocene paleofacies evolution of the Arabian Plate and its hydrocarbon occurrences. *GeoArabia* 6 (3).
- Zeyen, H., Volker, F., Wehrle, V., Fuchs, K., Sobolev, S.V., Altherr, R., 1997. Styles of continental rifting: crust-mantle detachment and mantle plumes. *Tectonophysics* 278 (1), 329–352.
- Mantle Plumes, 2017. <http://www.mantleplumes.org/CompleteHotspot.html>. (Accessed 6 November 2017).